CVEL

THE CLEMSON UNIVERSITY VEHICULAR ELECTRONICS LABORATORY

TECHNICAL REPORT: CVEL-10-020

Calculating Radiated Emissions due to I/O Line Coupling on Printed Circuit Boards using the Imbalance Difference Method

Changyi Su and Dr. Todd Hubing
Clemson University

April 4, 2011

This report was submitted for publication. The revised, peer-reviewed version can be found in the following publication:

C. Su and T. Hubing, "Calculating radiated emissions due to I/O line coupling on printed circuit boards using the imbalance difference method," *IEEE Trans. on Electromagnetic Compatibility*, vol. 54, no. 1, Feb. 2012, pp. 212-217.

Table of Contents

Abstract

High frequency signals on printed circuit board traces can couple to input/output (I/O) nets that carry the coupled energy away from the board and result in significant radiated emissions. A modeling technique is proposed to speed up the analysis of printed circuit boards (PCBs) with coupled microstrip lines that induce common-mode currents on attached cables. Based on the concept of imbalance difference, differential-mode sources are converted to equivalent common-mode sources that drive the attached cable and the PCB reference plane. A closed-form expression based on the imbalance difference model is developed to estimate the maximum radiated emissions due to I/O line coupling in PCBs.

1. Introduction

Crosstalk is a major concern for PCB designers. Coupling between signal lines can cause electromagnetic interference (EMI) issues as well as signal integrity (SI) problems. Crosstalk between signal traces and traces that connect to wires that bring signals or power onto the board (I/O lines) can be particularly troublesome. Although crosstalk can be minimized by careful rooting of signal and I/O traces, there are times when a designer has no alternative but to allow some amount of crosstalk in their design. Calculating levels of crosstalk is particularly challenging when one of traces is an I/O trace, because the termination impedance of the trace may be unknown.

One approach for analyzing the radiated emissions due to coupling between signal and I/O lines in a PCB is through simulation of the interconnect system using a 3D full-wave electromagnetic modeling (EM) simulator. Full-wave models can provide accurate solutions to well-defined problems, but they require significant computational resources and they cannot predict how small changes in the structure will affect the results without repeating the analysis with these changes made. Full-wave models are not practical option for providing fast estimates of worst-case radiated emissions during the initial design and routing processes. An alternative approach is to divide the entire I/O coupling problem into three essential components:

1. Calculating the voltages coupled to the I/O line circuit;
2. Modeling the wire/board structure as an antenna;
3. Determining the maximum radiated emissions from this source/antenna structure.

Extensive research has been devoted to developing fast and accurate techniques for crosstalk analysis [1]-[4], the first component of this problem. Less research has been done on the antenna model and the radiated emission estimation, but simple equations were derived by assuming the attached cable was an isotropic radiator in [5]. A maximum radiated field estimate based on a dipole antenna model was presented in [6]-[9]. In this model, a common-mode voltage source was applied between the cable and the PCB reference plane at the connector; but the input impedance of the antenna was required to determine the magnitude of the common-mode voltage. In the previous papers, either simulations [7]or measurements [8]were used to obtain the impedance of the antenna. In [9], a worst-case estimate of the antenna impedance, based on a resonant half-wave dipole, was used. This method did not require simulation or measurement of the input impedance of the antenna and provided a reasonable estimate of the worst-case radiated emissions. However, it did not calculate the field strength at frequencies between the resonances. Finally, the effects of eliminating the coupled lines and the dielectric layer from the antenna model were also unclear. An equivalent model which includes the I/O line and part of the dielectric layer was proposed in [10]. However, these details significantly increased the simulation time.

In Section 2, the Thevenin equivalent source coupled to the I/O circuit is determined. Section 3 introduces a model for calculating the radiated emissions due to I/O coupling on PCBs that significantly reduces simulation times without sacrificing the accuracy of the results. The model is derived based on the concept of imbalance difference [11]-[15]. The differential-mode signals on the signal traces are converted to equivalent common-mode sources quantitatively using a parameter called the imbalance factor. In the imbalance difference model, the lines carrying differential signals on the PCB are replaced by equivalent common-mode sources. This model separates the radiation problem from the PCB coupling problem and provides a fast way to estimate the radiated fields from the PCB due to coupling between signal and I/O lines. In Section 4, a closed-form expression is developed based on the imbalance difference model to predict the maximum radiation from the PCB. The accuracy of the model and the closed-form expression are evaluated for various test geometries in Section 5.

2. Thevenin Equivalent Coupling Source

A schematic illustrating the coupling from a high-speed signal trace to an adjacent I/O line is shown in Fig. 1. The signal trace and the I/O line are routed next to each other over a wide ground plane. The traces are on the same layer without conducting planes between them. The signal trace is connected to a signal source at one end and terminated with a load at the other end. The I/O trace is terminated with a resistance at the near-end and a wire extending beyond the return plane at the far-end. The signal can be coupled to the I/O circuit by two coupling mechanisms: magnetic-field coupling or electric-field coupling. Magnetic-field (or inductive) coupling occurs when the magnetic field lines from the source circuit, pass through the loop formed by the I/O trace circuit and return plane. Schematically, magnetic coupling is represented by a mutual inductance (L_m) between the two loops. Similarly, a mutual capacitance (C_m) between the two traces is used to indicate that energy is coupled from the source circuit to the victim circuit through an electric field (i.e. capacitive coupling).

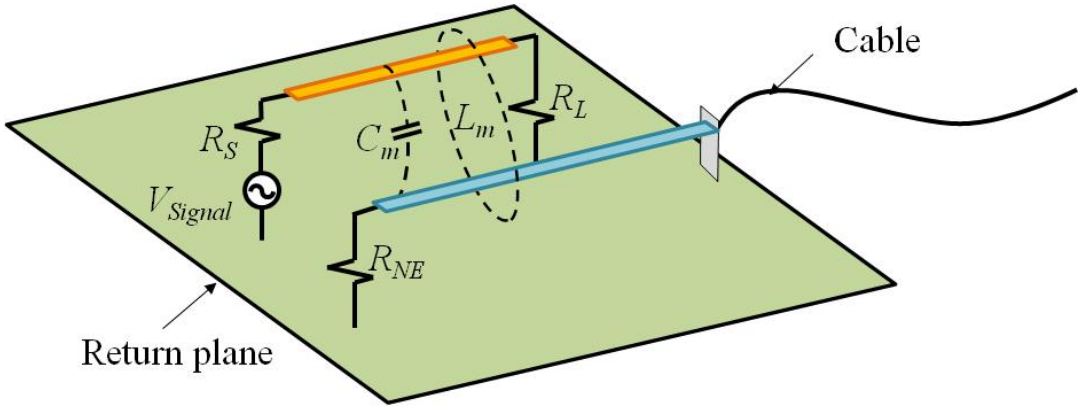

Fig. 1. Schematic representation of signal coupling to an I/O line.

In this paper, the analysis of this problem will be broken into three distinct stages:

1. Developing the equivalent lumped-element circuit model for the two coupling mechanisms and determining the total voltage coupled to the victim circuit;
2. Developing a relative simple imbalance difference model for the complex geometry;
3. Analyzing the simplified model to determine either the actual or worst-case radiated emissions.

To calculate the crosstalk between the coupled lines, consider the equivalent circuit shown in Fig. 2. A source circuit consists of a source voltage (V_{signal}) and a source impedance (Z_S) which is connected to a load (Z_L) via a signal trace. Two other terminations, denoted as Z_{NE} and Z_{FE}, are connected to an I/O trace. The circuit terminations are known and have variable values, with the exception of the far-end load of the I/O trace (Z_{FE}), where the cable is attached. The equivalent impedance looking into the attached cable is actually the input impedance of an antenna which is driven by the induced voltage at the connector.

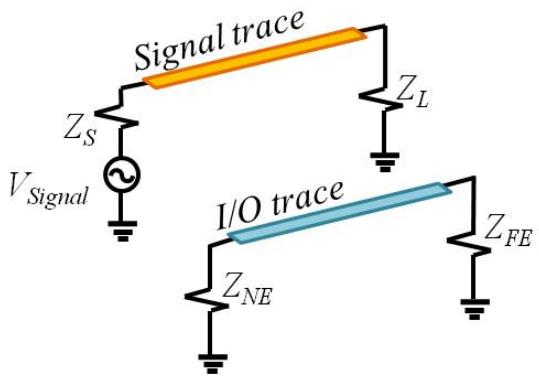

Fig. 2. Equivalent circuit illustrating crosstalk.

Two types of coupling induce noise in the victim circuit, i.e. the inductive coupling and the capacitive coupling. By assuming the lines are weakly coupled, the total coupling is a linear combination of contributions due to these two coupling mechanisms [3]. In Fig. 3, the I/O trace and return plane is represented as a transmission line of length l. One end of the transmission line is connected to a voltage source (V_{ind}) which represents the induced *EMF* due to inductive coupling.

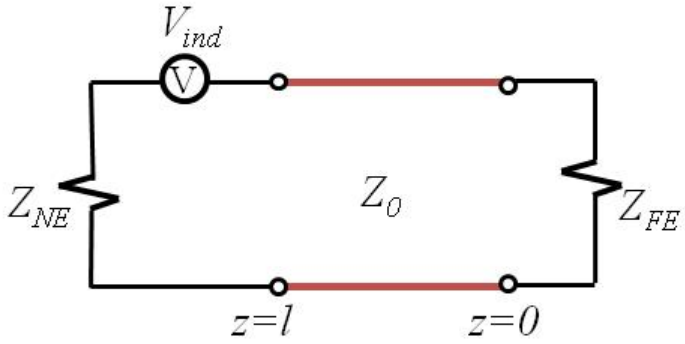

Fig. 3. The magnetic coupling model of the victim circuit.

By assuming the signal trace is electrically short, the induced voltage due to inductive coupling is given by

$$\hat{V}_{ind} = -j\omega L_m \frac{1}{Z_S + Z_L} \hat{V}_{Signal} \tag{1}$$

where L_m is the mutual inductance between the signal trace circuit and the I/O trace circuit.

In Fig. 4, an independent current source (I_{cap}) represents the induced current due to capacitive coupling.

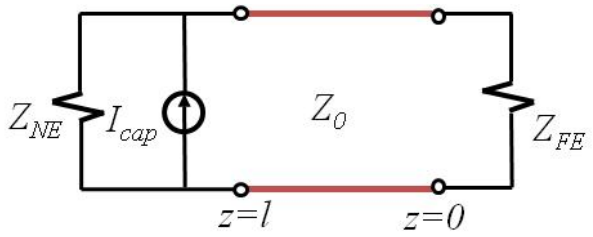

Fig. 4. The capacitive coupling model of the victim circuit.

The induced current source amplitude is

$$\hat{I}_{cap} = j\omega C_m \frac{Z_L}{Z_S + Z_L} \hat{V}_{Signal} \tag{2}$$

where C_m is the mutual capacitance between the signal trace circuit and the I/O trace circuit.

The total voltage induced in the victim circuit is the linear superposition of the two equivalent coupling sources,

$$\begin{aligned} \hat{V}_{total} &= \hat{V}_{ind} + \hat{V}_{cap} \\ &= j\omega \left[-L_m \frac{1}{Z_S + Z_L} + C_m \frac{Z_{NE} Z_L}{Z_S + Z_L} \right] \hat{V}_{Signal} \end{aligned} . \tag{3}$$

At low frequencies, the I/O trace can be approximated as lossless transmission line and the voltage at the connector is readily calculated from transmission line theory [16]. As shown in Fig. 5(a), the I/O line structure in Fig. 1 is represented as a transmission line of length *l* connected on one end to a source circuit and on the other end to a load (Z_{FE}). The circuit in Fig. 5(b) is the Thevenin equivalent of the circuit in Fig. 5(a).

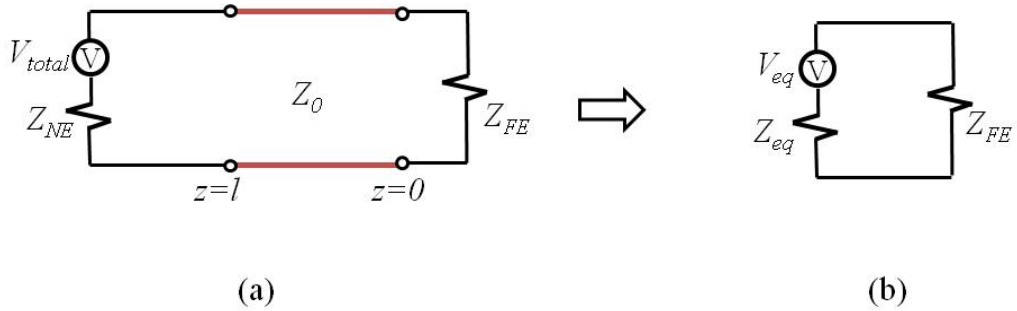

Fig. 5. Equivalent circuits for the I/O line structure, (a) transmission line circuit, (b) Thevenin equivalent circuit.

The Thevenin equivalent source driving Z_{FE} consists of an equivalent voltage source (V_{eq}) and equivalent impedance (Z_{eq}). The general solution for voltage on a lossless transmission line is

$$\hat{V}(z) = V_0^+ e^{-j\beta z} + V_0^- e^{j\beta z}, \tag{4}$$

where V_0^+ and V_0^- are the voltage amplitudes of the incident and reflected waves, respectively. The Thevenin voltage for the circuit in Fig. 5(a) is

$$\hat{V}_{eq} = \hat{V}_{total}(z=0) = V_0^+ + V_0^- = V_0^+ (1+\Gamma) . \tag{5}$$

When calculating the open-circuit voltage, the reflection coefficient is one since the load side is open. Therefore, Eq. (5) becomes

$$\hat{V}_{eq} = V_0^+ + V_0^- = 2V_0^+ . \tag{6}$$

where V_0^+ is given by

$$V_0^+ = \left(\frac{\hat{V}_{total} Z_{in}}{Z_{in} + Z_{NE}} \right) \left(\frac{1}{e^{j\beta l} + e^{-j\beta l}} \right) . \tag{7}$$

Z_{in} is the input impedance looking toward the open-circuit load and is given by

$$Z_{in} = \frac{Z_0}{j \tan \beta l} , \tag{8}$$

where Z_0 is the characteristic impedance of the transmission line and β is the wave number.

Combining Eq. (6) - (7), leads to the result

$$\hat{V}_{eq} = 2 \left(\frac{Z_0}{Z_0 + jZ_{NE} \tan \beta l} \right) \left(\frac{\hat{V}_{total}}{e^{j\beta l} + e^{-j\beta l}} \right) . \tag{9}$$

Replacing V_{total} with Eq. (3), the magnitude of $\hat{V}_{eq}$ is

$$\left| \hat{V}_{eq} \right| = \left| \frac{\hat{V}_{Signal}}{\cos \beta l} \right| \left| \frac{Z_0}{Z_0 + jZ_{NE} \tan \beta l} \right| \left| -\omega L_m \frac{1}{Z_S + Z_L} + \omega C_m \frac{Z_{NE} Z_L}{Z_S + Z_L} \right| . \tag{10}$$

The Thevenin equivalent impedance is

$$Z_{eq} = Z_0 \left(\frac{Z_{NE} + jZ_0 \tan \beta l}{Z_0 + jZ_{NE} \tan \beta l} \right) . \tag{11}$$

The mutual inductance and capacitance in Eq. (10) can be calculated based on the concept of even-mode and odd-mode capacitances of coupled microstrip lines on a printed circuit board [17].

3. The Imbalance Difference Model

In Section II, the complex geometry in Fig. 1 was simplified by removing the signal trace circuit and applying the total induced voltage source to the victim circuit, as shown in Fig. 6(a). The development of the simplified circuit in Fig. 6(a) does not require any prior knowledge of the impedance at the cable end of the I/O circuit. In this section, the structure in Fig. 6(a) is further simplified using the imbalance difference theory first proposed by Watanabe [11]and further developed in [12]-[15]. According to this theory, the common-mode current on the cable in Fig. 6(a) is equivalent to the current on the cable in Fig. 6(b). In Fig. 6(b), the ground plane is driven against the cable by two common-mode sources. The amplitude of each common-mode source is the product of the differential-mode voltage and the change in the imbalance factor that occurs at teach end of the I/O trace. Since the width of the trace is much smaller than that of the board, the change in the imbalance at the source end of the trace is very close to zero. Hence, the magnitude of the first common-mode source (V_{CM1}) is close to zero. The change in the imbalance factor at the other end is very close to 1. Therefore, the magnitude of the second common-mode source (V_{CM2}) is approximately equal to the differential-mode voltage (V_{FE}) at the connector. With thee approximations, the equivalent model in Fig. 6(b) can be further simplified to Fig. 6(c) in which the board is driven by the differential-mode voltage at the load end of the I/O trace.

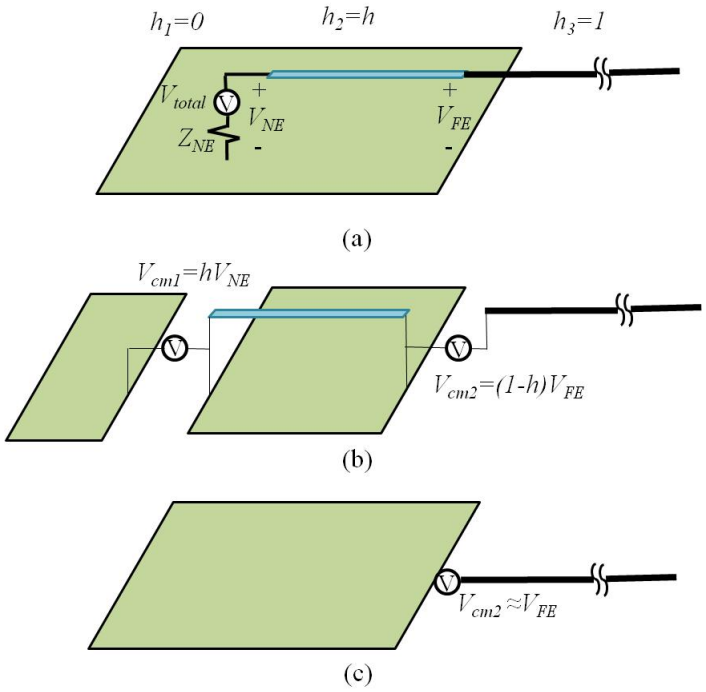

Fig. 6. The imbalance difference model for the I/O line structure, (a) full model (b) imbalance difference model (c) simplified imbalance difference model.

From the circuit in Fig. 6(c), the voltage driving the cable depends on the value of the antenna impedance. The input impedance of the dipole-type antenna in Fig. 6(c) is a complex function of frequency that can only be determined by full-wave simulation or measurement. To avoid doing this, the equivalent model in Fig. 6(c) is replaced by the model in Fig. 7. In the new model, the Thevenin equivalent source in Fig. 5(b) is substituted for the common-mode source in Fig. 6(c). For cable current calculations, the simplified source in Fig. 7 is equivalent to the original circuit in Fig. 1 and does not require any assumptions about the antenna input impedance.

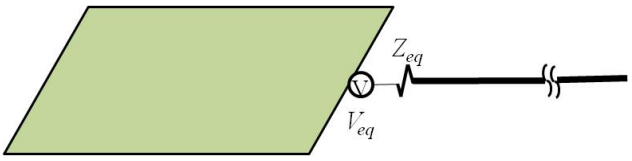

Fig. 7. Imbalance difference model.

In Fig. 7, both the I/O line and the dielectric layer were deleted from the model. While these play an important role in full-wave simulations of the entire structure, they are relatively unimportant after the amplitude of the common-mode source is determined. To achieve the highest degree of accuracy, they can be left in the model, but eliminating the I/O line and the dielectric layer from the equivalent model significantly reduces the simulation time while still yielding good results.

4. Maximum Radiated Emission Estimation

A full-wave analysis of the radiated emissions from the simplified model in Fig. 7 will yield virtually the same results as a full-wave analysis of the much more complex configuration in Fig. 1. However, very often for EMC problem analysis, it is much more useful to obtain the maximum emissions from the PCB with all possible cable lengths and orientations than it is to obtain the emission from one specific cable geometry. A closed-form formula was developed in [18]to estimate

the maximum radiated electric field from the antenna model in Fig. 7. This formula was enhanced in [19]to be more accurate over larger frequency ranges. When a board is driven by an ideal common-mode source, V_{CM}, the maximum electric field can be calculated as

$$|E|_{\max} \simeq \begin{cases} 20 \times I_{peak} \times \dfrac{2}{\sin\left(\sqrt{2}\right)} & f \le \dfrac{c_0}{l_{cable}} \\ 20 \times I_{peak} \times \dfrac{2}{\sin\left(\sqrt{\dfrac{c_0}{f l_{cable}}}\right)} & f > \dfrac{c_0}{l_{cable}} \end{cases}, \tag{12}$$

where l_{cable} is the length of the attached cable, f is the frequency, and c_0 is the propagation velocity in free space. I_{peak} is the highest current that actually exists on the cable and is given by

$$I_{peak} = \frac{V_{CM}}{\dfrac{R_{\min}}{board\_factor \times cable\_factor}}. \tag{13}$$

R_{min} is the input resistance of a resonant quarter-wave monopole. Two factors were defined to account for the effect that the finite cable length and the small board size have on this minimum resistance

$$board\_factor = \begin{cases} \sin\left(2\pi l_{board}/\lambda\right) & \text{when } l_{board} \le \dfrac{\lambda}{4} \\ 1.0, & \text{otherwise.} \end{cases}, \tag{14}$$

$$cable\_factor = \begin{cases} \sin\left(2\pi l_{cable}/\lambda\right) & \text{when } l_{cable} \le \dfrac{\lambda}{4} \\ 1.0, & \text{otherwise.} \end{cases}, \tag{15}$$

and

$$l_{board} = \frac{1 + 2L/W}{2L/W} \times \sqrt{L^2 + W^2},$$

where L and W denote the board length and width.

The common-mode source in Fig. 7 is connected to the equivalent impedance, Z_{eq}. Since this impedance value is not affected by the cable length and source location, the highest current on the cable can be written as

$$I_{peak} = \frac{V_{eq}}{\left| Z_{eq} + \dfrac{R_{\min}}{board\_factor \times cable\_factor} \right|}. \tag{16}$$

For the model in Fig. 7, Eqs. (12-16) can be used to estimate the maximum radiated electric field strength at a distance of 3 meter from the board.

5. Validation

In order to validate the equivalent model in Fig. 7, the radiated fields from various I/O coupling geometries were calculated using a full-wave numerical modeling code [20]. The modeled test board and the coupled traces are shown in Fig. 8. The test board has a dimensions L x W. The traces have a microstrip line structure. A cross-sectioned view of the coupled microstrip line structure is also shown

in Fig. 8.The signal trace is driven by a 1-V, 50-Ω voltage source at one end and terminated with a 50-Ω load at the other end. An I/O trace is routed parallel with the signal trace and extended beyond the board as 1 meter long cable with negligible diameter. The near-end of the I/O trace is terminated with a 50-Ω resistor. The space between the traces and the ground plane is filled with a dielectric material with a dielectric constant, ε_r.

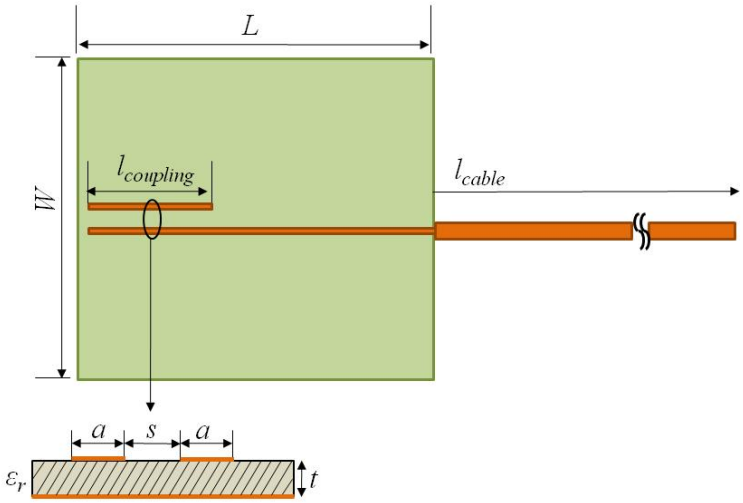

Fig. 8. Test geometry.

To validate the imbalance difference model and the closed-form expression in Eqs. (12-16), both the geometry and the dielectric constant were varied as listed in Table I. The geometrical parameters include the trace width-to-height ratio (*a/t*), the separation-to-height ratio (*s/t*), the coupling length, and the board width.

Table I. Simulation configurations

Test Case	Geometrical parameters					Dielectric constant ε_r
	a/h	*s/h*	$L_{coupling}$ (mm)	*L (mm)*	*W (mm)*	
1	0.5	0.5	20	100	100	1.0
2	0.5	1.0	20	100	100	1.0
3	1.0	0.5	20	100	100	1.0
4	0.5	0.5	40	100	100	1.0
5	0.5	0.5	20	100	40	1.0
6	0.5	0.5	20	100	100	4.0

Fig. 9 shows a plot of the simulation results from the model of the entire configuration and the corresponding imbalance difference model, together with the maximum emissions estimate for Case 1. The imbalance difference model yields results that are in good agreement with the original configuration over the entire 10-1000 MHz frequency range. The closed-form expression estimates the peak emissions from the board within a few dB at every resonant frequency. Figs. 10-13 show similar plots for test cases 2-5. In all cases, the difference between the simulation and the estimate is within a few dB.

In Case 6, where the dielectric constant is 4.0, the agreement between the full model (with dielectric) and the imbalance difference model (no dielectric) is excellent. This demonstrates that the presence of the dielectric is no longer required after the model has been simplified using the imbalance difference model. Eliminating the dielectric layer from the imbalance difference model significantly reduces the simulation time without sacrificing the accuracy of the results.

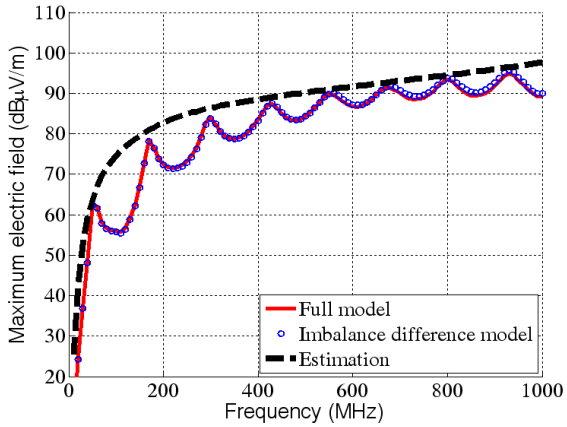

Fig. 9. Maximum radiation for Case 1.

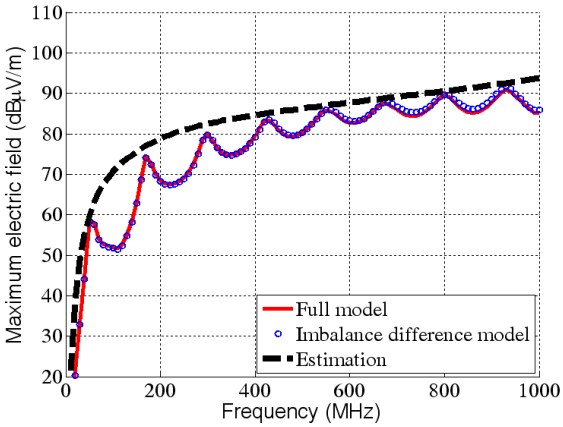

Fig. 10. Maximum radiation for Case 2.

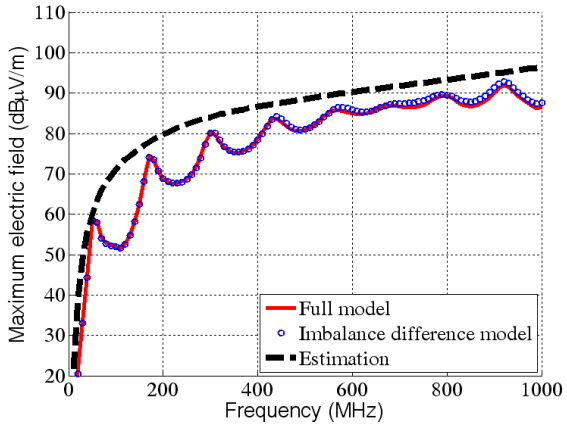

Fig. 11. Maximum radiation for Case 3.

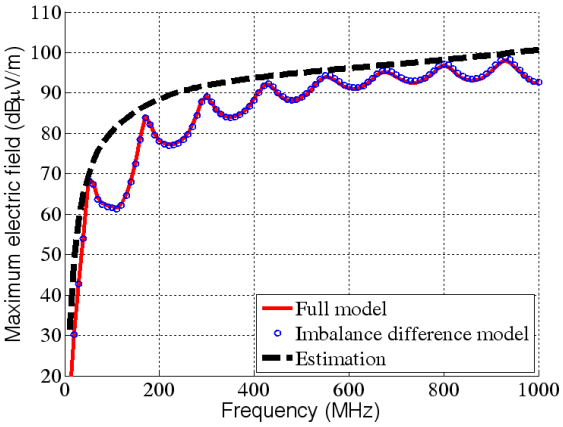

Fig. 12. Maximum radiation for Case 4.

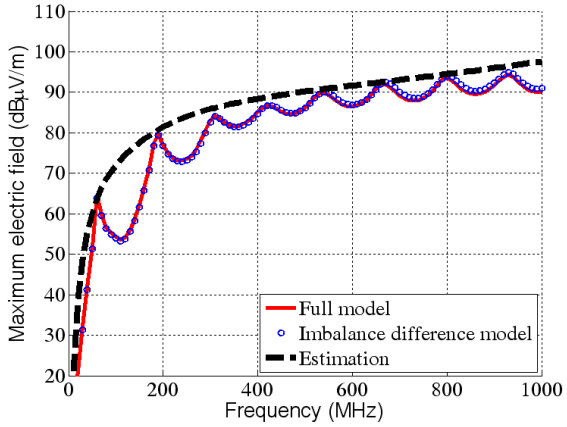

Fig. 13. Maximum radiation for Case 5.

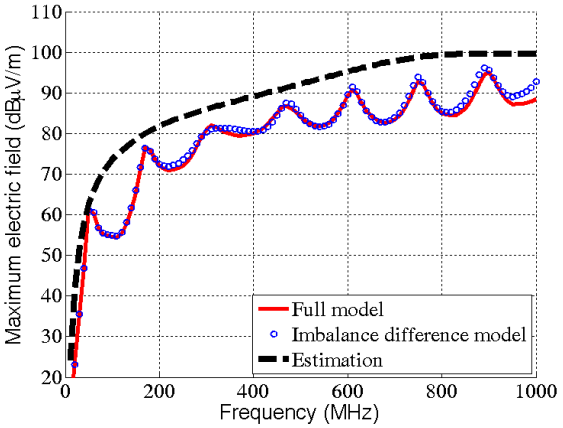

Fig. 14. Maximum radiation for Case 6.

6. Conclusions

An equivalent source/imbalance difference model for printed circuit boards with coupling between high-speed traces and I/O traces has been presented. In this model, the differential-mode sources and traces are replaced with a common-mode voltage source that drives the attached cable against the reference plane. The fine structures of the traces are eliminated in the equivalent model; and therefore, analysis of the equivalent model requires much less computational resources than an analysis of the full model. Based on the imbalance difference model, a closed-form expression was also presented that estimates the maximum radiated emissions from the PCB-cable structure.

References

[1] B. D. Jarvis, "The effects of interconnections on high-speed logic circuits," *IEEE Trans. Electron. Comput.*, vol. 12, pp. 476-487, Oct. 1963.

[2] J. A. DeFalco, "Predicting crosstalk in digital systems," *Comput. Design*, vol. 12, no. 6, pp. 69-75, June 1973.

[3] C. Paul, *Introduction to Electromagnetic Compatibility*, New York: John Wiley & Sons, Inc., 1992.

[4] C. R. Paul, *Analysis of Multiconductor Transmission Lines*, New York, NY: John Wiley & Sons, Inc., 1994.

[5] H. Shim, T. Hubing, T. Van Doren, R. DuBroff, J. Drewniak, D. Pommerenke, and R. Kaires, "Expert system algorithms for identifying radiated emission problems in printed circuit boards," in *Proc. 2004 IEEE Int. Symp. Electromagn. Compat.*, Santa Clara, CA, vol. 1, Aug. 9–13, 2004, pp. 57-62.

[6] N. Oka, C. Miyazaki, and S. Nitta, "Radiation from a PCB with coupling between a low frequency and a digital signal traces," in *Proc. 1998 IEEE Int. Symp. Electromagn. Compat.*, Aug 1998, pp. 635-640.

[7] W. Cui, M. Li, J. Drewniak, T. Hubing, T. Van Doren, R. DuBroff and X. Luo, "Anticipating EMI from coupling between high-speed digital and I/O lines," in *Proc. 1999 IEEE Int. Symp. Electromagn. Compat.*, Seattle, WA, Aug. 1999, pp. 189-194.

[8] M. Tanaka, W. Cui, X. Luo, J. L. Drewniak, T. H. Hubing, T. P. Van Doren, R. E. DuBroff, "FDTD modeling of EMI antennas," in *Proc. 1999 IEEE Int. Symp. Electromagn. Compat.*, 1999, pp.560-563.

[9] W. Cui, H. Shi, X. Luo, J. L. Drewniak, T. P. Van Doren, and T. Anderson, "Lumped-element sections for modeling coupling between high-speed digital and I/O lines," in *Proc. 1997 IEEE Int. Symp. Electromagn. Compat.*, Austin, Texas, Aug., 1997, pp. 260-265.

[10] S. Ohtsu, K. Nahase, and T. Yamagajou, "Analysis of radiation caused by LSI package cross talk and cable by using the time-domain moment method," in *Proc. 2002 IEEE Int. Symp. Electromagn. Compat.*, Minneapolis, MN, Aug. 2002, pp. 268–272.

[11] T. Watanabe, O. Wada, T. Miyashita and R. Koga, "Common-mode-current generation caused by difference of unbalance of transmission lines on a printed circuit board with narrow ground pattern," *IEICE Transactions on Communications*, vol. E83-B, no. 3, March 2000, pp. 593-599

[12] T. Watanabe, S. Matsunaga, O. Wada, M. Kishimoto, T. Tanimoto, A. Namba, and R. Koga, "Equivalence of two calculation methods for common-mode excitation on a printed circuit board

with narrow ground plane," in *Proc. 2003 IEEE Symp. Electromagn. Compat.*, Boston, MA, Aug. 2003, pp. 22–27.

[13] Y. Toyota, T. Matsushima, K. Iokibe, R. Koga, T. Watanabe, "Experimental validation of imbalance difference model to estimate common-mode excitation in PCBs," in *Proc.2008 IEEE Int. Symp. Electromagn. Compat.*, Detroit, Aug. 2008, pp. 1-6.

[14] T. Matsushima, T. Watanabe, Y. Toyota, R. Koga, and O. Wada, "Prediction of EMI from two-channel differential signaling system based on imbalance difference model," in *Proc. 2010 IEEE Int. Symp. Electromagn. Compat*., Fort Lauderdale, July 2010, pp. 413-418.

[15] C. Su and T. Hubing, "Imbalance Difference Model for Common-mode Radiation from Printed Circuit Boards," *IEEE Trans. Electromagn. Compat.*, vol. 53, no. 1, Feb. 2011.

[16] D. M. Pozar, *Microwave Engineering*, New York, John Wiley & Sons Inc, 2005.

[17] K. C. Gupta, Ramesh Garg, Inder Bahl, and Prakash Bhartia, *Microstrip Lines and Slotlines, 2nd edition*, Artech House, Norwood, MA, 1996.

[18] S. Deng, T. Hubing and D. Beetner, "Estimating maximum radiated emissions from printed circuit boards with an attached cable," *IEEE Trans. Electromagn. Compat.*, vol. 50, no. 1, pp. 215-218, Feb. 2008.

[19] C. Su, and T. Hubing, "Improvements to a method for estimating the maximum radiated emissions from PCBs with cables," *CVEL Technical Report, CVEL-11-024*, March 2011.

[20] FEKO User's Manual, Suite 6.0, September 2010.